JOURNAL OF SOLID STATE CHEMISTRY 120, 121–127 (1995)

Preparation, Crystal Structure, Dielectric Properties, and Magnetic Behavior of $Ba_2Fe_2Ti_4O_{13}$

T. A. Vanderah,* Q. Huang,*† W. Wong-Ng,* B. C. Chakoumakos,‡ R. B. Goldfarb,§ R. G. Geyer,§ J. Baker-Jarvis,§ R. S. Roth,* and A. Santoro*

*National Institute of Standards and Technology, Gaithersburg, Maryland 20899; †University of Maryland, College Park, Maryland 20742; ‡Solid State Division, Oak Ridge National Laboratory, Oak Ridge, Tennessee 37831-6393; and §National Institute of Standards and Technology, Boulder, Colorado 80303

Received April 10, 1995; revised August 7, 1995; accepted August 8, 1995

The preparation, crystal structure, dielectric properties, and magnetic behavior of the new compound $Ba_2Fe_2Ti_4O_{13}$ are reported. Structural studies carried out by single-crystal X-ray diffraction and neutron powder diffraction show that this phase is isostructural with $K_2Ti_6O_{13}$ and $Ba_2ZnTi_5O_{13}$ ($C2/m$ (No. 12); $a = 15.216(1)$, $b = 3.8979(3)$, $c = 9.1350(6)$ Å, $\beta = 98.460(7)°$; $V = 535.90(8)$ Å^3; $Z = 2$). The cations Fe^{3+} and Ti^{4+} are partially ordered among distorted octahedral sites with Ba^{2+} occupying eleven-coordinated polyhedra. $Ba_2Fe_2Ti_4O_{13}$ exhibits TE_0 resonance near 10 GHz with a dielectric constant of ~28 and a dielectric loss tangent of 2×10^{-3}. The compound displays complex paramagnetic behavior with marked field dependence; the magnetization at 80 kA/m is several orders of magnitude smaller than that of most ferrites. Spin-glass effects have not been observed; however, weak collective interactions are clearly present. No magnetic ordering has been detected by neutron diffraction down to 13 K. © 1995 Academic Press, Inc.

INTRODUCTION

Barium polytitanates are used in many practical applications, such as dielectric ceramic resonators in microwave communication devices operating in the 50 MHz to 20 GHz region. Ternary systems of BaO + TiO_2 with ZrO_2, Al_2O_3, MgO, Nb_2O_5, or ZnO have been fairly well characterized and many of the relevant phases have been examined crystallographically. A summary of the results obtained in these studies is given in Ref. (1). Dielectric ceramics that are also magnetic are widely used as coaxial circulators and isolators in communication systems, hence our interest in the BaO–Fe_2O_3–TiO_2 phase diagram. To our knowledge, prior to this work, only two ternary compounds in the BaO–Fe_2O_3–TiO_2 system have been characterized structurally, namely $Ba_{12}Fe_{28}Ti_{15}O_{84}$(2) and $BaFe_4Ti_2O_{11}$ (3, 4). In both cases the Fe^{3+} and Ti^{4+} cations were found to be distributed on the same crystallographic sites. The first compound was analyzed with X-ray single-crystal methods, and the occupancies of the two cations in each site could be determined in the structural refinement. The second compound was studied with X-ray and neutron powder diffraction techniques. The X-ray data were not sufficiently precise to carry out occupancy refinements and only the subsequent neutron powder diffraction study revealed the distribution of the two cations. Our present studies have established the existence of a number of other ternary phases, one of which is the title compound $Ba_2Fe_2Ti_4O_{13}$. The crystal structure has been first characterized by X-ray single-crystal techniques. Because of the large difference between the iron and titanium neutron scattering amplitudes (0.954 and -0.344×10^{-12} cm, respectively), neutron powder diffraction was then used to ascertain if these two cations are disordered over the same crystallographic sites and to determine precisely the values of their occupancy factors. Magnetization and dielectric measurements were carried out in view of possible practical applications of this material. The results of these investigations are described in the following sections of the paper.

EXPERIMENTAL

A. Sample Preparation

Polycrystalline $Ba_2Fe_2Ti_4O_{13}$ was prepared by solid-state reaction of stoichiometric quantities of reagent grade $BaCO_3$, Fe_2O_3, and phosphate-free TiO_2 in air. Before each heating the sample was ground 15 min with an agate mortar and pestle, pelletized, and placed on a bed of sacrificial powder of the same composition in an alumina combustion boat. The sample was first heated to 1000°C for 27 hr and then twice at 1250°C for 166 and 186 hr. Sample purity was confirmed by X-ray powder diffraction, using Cu$K\alpha$ radiation. All the observed peaks could be indexed on the basis of a unit cell similar to that of $Ba_2ZnTi_5O_{13}$ (1, 5), suggesting that the two compounds are isostructural. Single crystals of $Ba_2Fe_2Ti_4O_{13}$ were obtained as a minor product from a partial melt of the compound $BaFe_4Ti_2O_{11}$:

0022-4596/95 $12.00

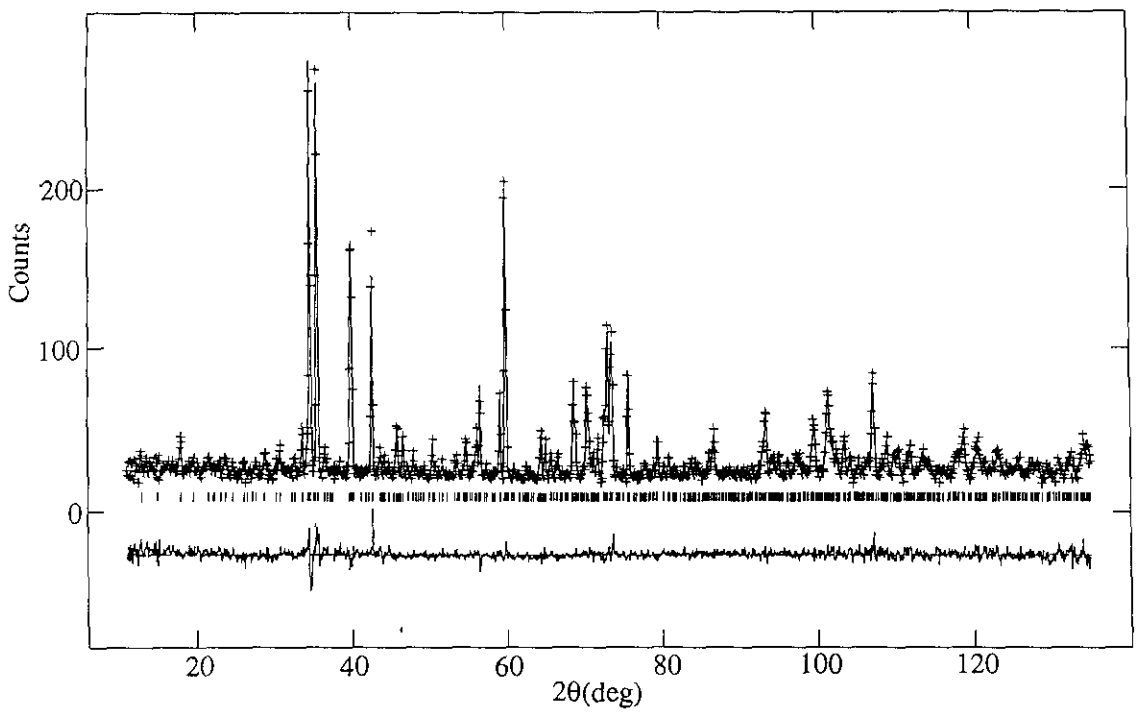

FIG. 1. Plot of the observed (crosses) and calculated (continuous line) intensities in the neutron powder diffraction pattern of $Ba_2Fe_2Ti_4O_{13}$. The differences between observed and calculated intensities are plotted at the bottom of figure.

a powder of this material was heated in a platinum capsule in air at 1390°C for 4 hr, cooled at 2°/hr to 1180°C, furnace cooled to 750°C, and then removed from the furnace. Red single crystals of the title compound were identified and characterized by the precession method using Zr-filtered Mo$K\alpha$ radiation prior to structure determination.

B. Diffraction Measurements and Structural Refinements

X-ray single-crystal intensities were collected from a plate-like crystal mounted inside a Lindemann glass capillary in a random orientation, using a computer controlled kappa-axis diffractometer equipped with a graphite monochromator. Cell constants and the orientation matrix were obtained by least-squares methods from the setting angles of 25 reflections in the angular range $12° < \theta < 23°$. The results of these measurements and other details about the intensity data collection are summarized in Table 1a. Three standard reflections used for monitoring the stability of the crystal showed negligible variation in intensity. A total of 1995 reflections were collected up to $2\theta = 76°$, of which 1628 were unique. Of these, 1433 had $F^2 \geq 3\sigma(F^2)$ and were used in the structural refinements. The measured intensities were corrected for Lorentz and polarization effects and for absorption, using a semiempirical absorption correction evaluated by means of the psi-scan technique. The atomic scattering factors used in all refinements were those given by Cromer and Waber (6). The structure was successfully refined by assuming isomorphism with $Ba_2ZnTi_5O_{13}$(1). In the preliminary calculations, ordering of the Fe^{3+} and Ti^{4+} was assumed, with the iron ions located at (0.76, 0.0, 0.23) and the titanium ions at (0.67, 0.5, 0.44) and (0.62, 0.5, 0.09). In the subsequent refinements, however, the two cations were distributed over these three crystallographic sites with occupancies fixed at the values determined in the neutron experiment (vide infra). The final atomic coordinates and anisotropic temperature factors obtained from the X-ray data are listed in Table 2.

The neutron powder diffraction measurements were made using the HB4 high-resolution powder diffractometer at the high flux isotope reactor at Oak Ridge National Laboratory, adopting the experimental conditions listed in Table 1b. Complete diffraction scans were obtained at room temperature and at 13 K. All refinements were carried out with the Rietveld method employing the program GSAS written by Larson and Von Dreele (7). The structure was refined assuming the symmetry of space group $C2/m$ and using as initial parameters those obtained in the first stages of the X-ray single-crystal experiment. A model with the iron and titanium cations ordered as in the initial stages of the X-ray refinement resulted in temperature factors abnormally high. In all subsequent calculations, therefore, these cations were distributed at random over the three M sites (M = Ti/Fe) and their occupancies were refined together with the positional and

TABLE 1a
Collection of X-Ray Single-Crystal Data for $Ba_2Fe_2Ti_4O_{13}$ at 295 K

Crystal dimensions	$0.18 \times 0.10 \times 0.03$ mm^3
MoKα radiation	0.71073 Å
Temperature	~295 K
Space group	*C2/m* (No. 12)
Cell parameters	$a = 15.216(1)$ Å, $b = 3.8979(3)$ Å, $c = 9.1350(6)$ Å, $\beta = 98.460(7)°$, $V = 535.90(8)$ Å^3
Z	2
Intensity collection	$\omega/2\theta$ scan
Data range	$0 < h < 26$, $-1 < k < 6$, $-15 < l < 15$

TABLE 1b
Collection of Neutron Powder Intensity Data

Monochromatic beam	115 reflection of Ge monochromator
Wavelength	1.417(1) Å
Horizontal divergences	12′, 20′, 6′ of arc for the in-pile, monochromatic beam, and *diffracted beam collimators*, respectively
Sample container	Vanadium can with 9 mm diameter
2θ angular range	*11°–135°, steps: 0.05°*
Scattering amplitudes (10^{-12} cm)	b(Ba) = 0.525, b(Fe) = 0.954, b(Ti) = −0.344, b(O) = 0.581

thermal parameters of all the atoms in the unit cell, with only the constraint of full occupancy of each site. In order to reduce the number of variables, in the final refinement based on the room temperature neutron data the positional parameters of all the cations were kept fixed at the very precise values obtained in the X-ray analysis. Since atoms $M(1)$, $M(2)$, and $M(3)$ all have octahedral coordination, their thermal factors were constrained to be equal and were kept fixed at a value of 0.4 Å^2, close to the average of the corresponding X-ray results. Similarly, the thermal parameters of O(1), O(2), and O(4) were constrained to be equal due to the fact that these atoms have similar environments. The results of these calculations are listed in Table 2, and in Table 3 are given the relevant bond distances and valences calculated from the room temperature neutron results. The agreement between observed and calculated intensities is shown in the plot of Fig. 1, together with the difference I(obs)—I(cal) at the bottom of the figure.

As shown in Table 2, the agreement between X-ray and neutron positional parameters of the oxygen atoms is generally good. The occupancies of the Ti and Fe sites indicate a composition very close to that corresponding to the chemical formula of the compound. This good agreement is certainly due to the large difference in the scattering amplitudes of Ti and Fe. No phase transitions or magnetic reflections were observed down to a temperature of 13 K, showing that no long range magnetic ordering is present in the structure.

C. Characterization of Dielectric and Magnetic Properties

Permittivity and dielectric loss tangent measurements of a sintered pellet of polycrystalline $Ba_2Fe_2Ti_4O_{13}$ were performed at ambient temperature using a reentrant cavity (8) in the 100 MHz to 1 GHz region and a dielectric resonator configuration (9) in the 1 to 10 GHz region. Corrections to crystallographic density were incorporated by estimating the pore volume of the sample (from size and mass) and applying the Bruggeman effective medium formulation (10) for a two-phase composite. The uncertainties in the measurements of relative permittivities are ±1% and ±0.2%, respectively, for the reentrant cavity and dielectric resonator configurations; however, inaccuracy in the measurement of pore volume suggests a realistic accuracy level for the permittivity values of ±10%.

The magnetic properties of polycrystalline $Ba_2Fe_2Ti_4O_{13}$ were characterized using a commercial magnetometer equipped with a superconducting quantum interference device (SQUID). Mass magnetization was measured as a function of temperature (300–1.75 K) at low fields (±80 kA/m) and high fields (±5.6 MA/m). (Applied field values in units of A/m are converted to Oe by multiplying by $4\pi/10^3$; magnetization values in units of A · m^2/kg and emu/g are numerically equal (11).) To characterize hysteresis effects, low-field mass susceptibility (calculated as mass magnetization divided by applied field) was measured as a function of increasing temperature after zero-field cooling (ZFC) and field cooling (FC). For the ZFC data the sample was ac demagnetized at room temperature before cooling to 1.75 K.

DISCUSSION

A. Crystal Structure

As mentioned previously, the compound $Ba_2Fe_2Ti_4O_{13}$ is isostructural with $K_2Ti_6O_{13}$ and $Ba_2ZnTi_5O_{13}$. The projection of the structure along the unique b axis of the monoclinic system is shown in Fig. 2. The overall packing of the atoms can be described in terms of repeating units formed by three edge-sharing MO_6 octahedra. Each of these units is connected by corner-sharing to three similar units located on the same layer parallel to the a,c plane (e.g., at O(1), O(3′), and O(1′) in Fig. 2), forming double chains which run in the direction of the c axis. The chains are stacked on top of each other along the b axis with a zig-zag arrangement and in such a way that the octahedra of contiguous layers share edges, giving a structure in which

TABLE 2
Structural Parameters of $Ba_2Fe_2Ti_4O_{13}$ at 296 K (Neutron Powder Diffraction, First Line, and X-Ray Single Crystal, Second Line) and at 13 K (Neutron Powder, Third Line)

Space group: $C2/m$, a = 15.2074(4) Å, b = 3.89384(8) Å, c = 9.1305(2) Å, β = 98.471(2)°,
15.216(1) Å, 3.8979(3) Å, 9.1350(6) Å, 98.460(7)°,
15.1856(5) Å, 3.8917(1) Å, 9.1233(3) Å, 98.411(1)°,
V = 534.56(4) Å^3, Z = 2. R_p = 5.15, R_{wp} = 5.91, χ^2 = 1.38.
535.90(8) Å^3, R = 2.5, R_w = 3.5, R_r = 3.2.[a]
533.37(4) Å^3, R_p = 5.29, R_{wp} = 6.25, χ^2 = 1.39.

Atom	Position	x	y	z	B(Å^2)	Occupany
Ba	4*i* *m*	0.45079[b]	0	0.22909	0.8(1)	1
		0.45079(1)	0	0.22909(2)	0.725(3)	1
		0.4507(3)	0	0.2279(5)	0.23(9)	1
Ti(1)/Fe(1)	4*i* *m*	0.66916	1/2	0.43909	0.4[c]	0.906(5)/0.094(5)
		0.66916(3)	1/2	0.43909(6)	0.384(7)	0.906(5)/0.094(5)[d]
		0.6692(7)	1/2	0.441(1)	0.3(2)	0.911(6)/0.089(6)
Ti(2)/Fe(2)	4*i* *m*	0.61973	1/2	0.09422	0.4	0.613(6)/0.387(6)
		0.61973(3)	1/2	0.09422(6)	0.492(7)	0.613(6)/0.387(6)
		0.618(1)	1/2	0.100(2)	0.3(2)	0.628(6)/0.372(6)
Ti(3)/Fe(3)	4*i* *m*	0.75937	0	0.22905	0.4	0.487(6)/0.513(6)
		0.75937(3)	0	0.22905(5)	0.438(6)	0.487(6)/0.513(6)
		0.7572(5)	0	0.233(1)	0.3(2)	0.478(7)/0.522(7)
O(1)	4*i* *m*	0.3351(3)	1/2	0.0846(6)	0.50(5)	1
		0.3336(2)	1/2	0.0873(3)	0.75(3)	1
		0.3338(3)	1/2	0.0847(5)	0.10(8)	1
O(2)	4*i* *m*	0.5732(3)	1/2	0.3000(6)	0.50	1
		0.5714(2)	1/2	0.3001(3)	0.63(3)	1
		0.5718(3)	1/2	0.3007(6)	0.19(8)	1
O(3)	2*a* 2/*m*	1/2	1/2	0	0.7(2)	1
		1/2	1/2	0	0.80(5)	1
		1/2	1/2	0	0.7(1)	1
O(4)	4*i* *m*	0.3694(3)	1/2	0.3826(6)	0.50	1
		0.3707(2)	1/2	0.3826(3)	0.72(3)	1
		0.3694(3)	1/2	0.3819(6)	0.27(9)	1
O(5)	4*i* *m*	0.7394(3)	1/2	0.2410(6)	0.25(6)	1
		0.7382(2)	1/2	0.2423(3)	0.55(3)	1
		0.7391(3)	1/2	0.2426(6)	0.18(9)	1
O(6)	4*i* *m*	0.3641(3)	0	−0.1139(6)	0.25(9)	1
		0.3653(2)	0	−0.1133(3)	0.71(3)	1
		0.3643(3)	0	−0.1144(6)	0.13(8)	1
O(7)	4*i* *m*	0.2981(3)	0	0.5714(6)	0.25(6)	1
		0.2988(2)	0	0.5699(3)	0.47(3)	1
		0.2985(3)	0	0.5698(6)	0.30(7)	1

[a] Based on structure factors. R_r is the unweighted R factor including the unobserved reflections.
[b] The coordinates of the cations at 296K were fixed at the values obtained in the X-ray experiment.
[c] The temperature factors of Ti and Fe were fixed in the refinement.
[d] The occupancies of Ti and Fe were fixed at the values obtained in the neutron experiment at R.T.

no unshared corners are left. This arrangement of the MO_6 octahedra creates open channels parallel to the b and to the c axes, in which the barium cations are located.

As shown by the bond distances listed in Table 3, the MO_6 octahedra are highly distorted. More specifically, the M cations are displaced from the centers of the octahedra in the direction of the open sites where the Ba cations are located, while the Ba cations are shifted away from the centers of distorted cubes toward the contiguous empty cubic sites, as indicated by the arrows in Fig. 2. Part of these distortions are certainly due to the fact that Fe^{3+} and Ti^{4+} cations are disordered over the same M sites. However, this disordering cannot be the only factor playing a role in this case because a similar pattern of atomic shifts was observed also in the isostructural compound $K_2Ti_6O_{13}$(12). An explanation for the observed structure has been proposed by Cid-Dresdner and Buerger (12) who have argued that the acentric positions of the cations within

TABLE 3
Selected Bond Distances (Å) and Valences V (v.u.) of $Ba_2Fe_2Ti_4O_{13}$ at 296 K Calculated from the Results Reported in the First Lines of Table 2

Ba–O(1)	×2	2.811(6)	O(1)–*M*(3)		1.93(1)
Ba–O(2)	×2	2.707(5)	*V*(O(1))		2.01
Ba–O(3)	×2	3.024(4)			
Ba–O(4)	×2	2.797(5)	O(2)–Ba	×2	2.707(5)
Ba–O(5)		3.234(7)	O(2)–*M*(1)		1.80(1)
Ba–O(6′)		3.204(9)	O(2)–*M*(2)		2.11(2)
Ba–O(6)		3.148(6)	*V*(O(2))		2.10
V(Ba)		2.19			
			O(3)–Ba	×4	3.023(4)
M(1)–O(2)		1.80(1)	O(3)–*M*(2)	×2	1.90(2)
M(1)–O(4)		1.83(1)	*V*(O(3))		2.05
M(1)–O(5)		2.21(2)			
M(1)–O(7)	×2	2.009(3)	O(4)–B(a)	×2	2.797(5)
M(1)–O(7′)		2.13(1)	O(4)–*M*(1)		1.83(1)
V(*M*(1))/expected *V*(*M*(1))[a]		3.90/3.92	O(4)–*M*(3)		2.03(1)
			V(O(4))		1.98
M(2)–O(1)		1.86(2)			
M(2)–O(2)		2.11(2)	O(5)–Ba		3.234(7)
M(2)–O(3)		1.90(2)	O(5)–*M*(1)		2.21(2)
M(2)–O(5)		2.09(3)	O(5)–*M*(2)		2.09(3)
M(2)–O(6)	×2	1.968(3)	O(5)–*M*(3)	×2	1.967(2)
V(*M*(2))/expected *V*(*M*(2))		3.71/3.61	*V*(O(5))		2.10
M(3)–O(1)		1.93(1)	O(6)–Ba		3.204(9)
M(3)–O(4)		2.03(1)	O(6)–Ba		3.148(6)
M(3)–O(5)	×2	1.967(2)	O(6)–*M*(2)	×2	1.968(2)
M(3)–O(6)		1.99(2)	O(6)–*M*(3)		1.99(2)
M(3)–O(7)		2.08(1)	*V*(O(6))		2.01
V(*M*(3))/expected *V*(*M*(3))		3.45/3.49			
			O(7)–*M*(1)	×2	2.009(3)
O(1)–Ba	×2	2.811(6)	O(7)–*M*(1)		2.13(1)
O(1)–*M*(2)		1.86(2)	O(7)–*M*(3)		2.08(1)
			V(O(7))		2.04

[a] In these calculations Ti^{4+} and Fe^{3+} were assumed, and *M*(1): 91% Ti + 9% Fe, *M*(2): 61% Ti + 39% Fe, and *M*(3): 49% Ti + 51% Fe.

their coordination polyhedra are necessary to achieve electrical neutrality. This conclusion is consistent with the results of bond-length, bond-strength calculations carried out with the formalism and the parameters given by Brese and O'Keeffe (13), using the bond distances listed in Table 3 for the neutron refinement at room temperature and the observed occupancies. The valences at the cation sites and at the anion sites calculated with this procedure are shown in Table 3, where they are compared with their formal oxidation states. The agreement is generally very good and it shows that the combined shifts of the cations and anions from the positions they would occupy in an idealized structure made of regular octahedra result in quite reasonable valences for all the atoms in the unit cell. The greatest discrepancy between expected and calculated values is observed for barium (2.00 versus 2.19 v.u.). The difference of 0.19 v.u. may be due to underestimating one or more of the Ba–O distances or to uncertainties in the value of the R_{Ba-O} parameter. This last possibility is corroborated by the fact that values different from 2.00 v.u. are obtained for barium also in other compounds. For example, if we consider the Ba–O distances determined in one of the best refinements of the structure of $YBa_2Cu_3O_7$ (14), we obtain a Ba valence of 2.24 v.u. Values even larger than this are calculated for the twelve coordinated Ba cations in the compound $Ba_{12}Fe_{28}Ti_{15}O_{84}$ (2).

The Ba cations in $Ba_2Fe_2Ti_4O_{13}$ are eleven-coordinated, with coordination polyhedra which can be described as three-capped quadrilateral prisms. There are eight short Ba–O distances, ranging from 2.70 to 3.02 Å, with oxygen atoms located at the corners of a distorted cube and three long distances of 3.15, 3.20, and 3.23 Å with oxygen atoms O(6), O(6′), and O(5′), respectively. These last three atoms have been included in the coordination sphere of Ba because they have significant Ba–O bonding interations, each of them giving a contribution of about 4–5% to the barium

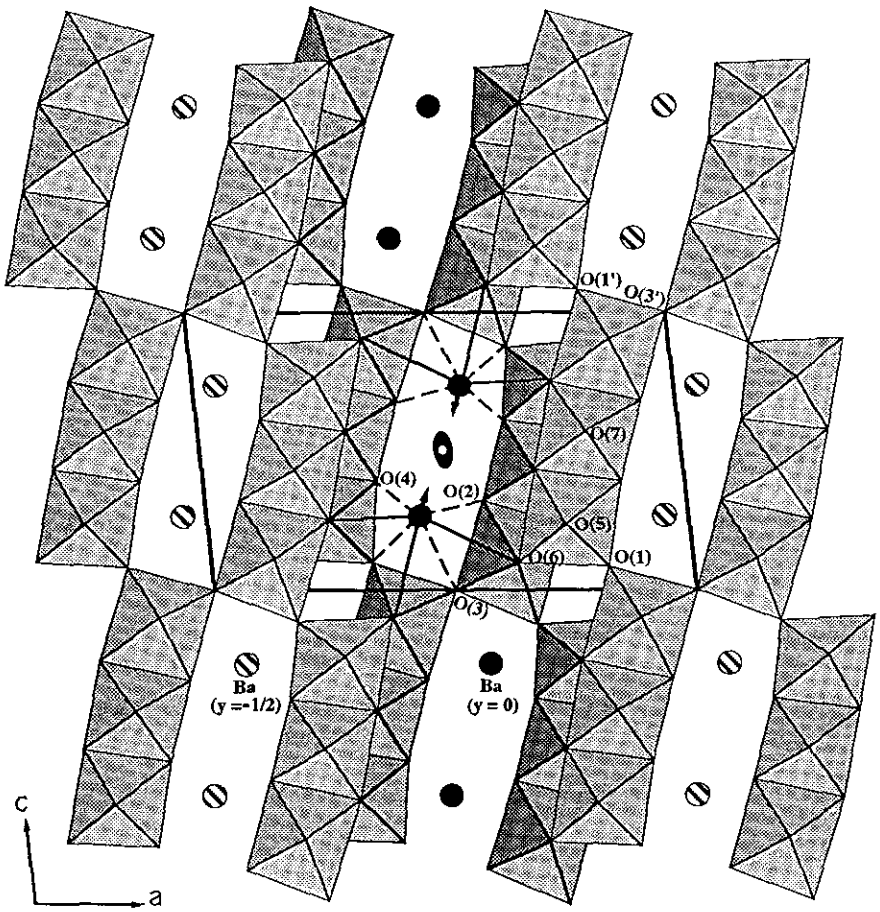

FIG. 2. Projection of the structure of $Ba_2Fe_2Ti_4O_{13}$ along the *b* axis of the monoclinic unit cell. The arrows indicate the shifts of the barium cations from the centers of distorted cubes.

valence. These distances agree well with those determined in related compounds containing iron and titanium (2). The *M*–O distances range from 1.80 to 2.21 Å, with average octahedral distances of 1.998, 1.983, and 1.994 Å for the *M*(1), *M*(2), and *M*(3) octahedra, respectively. Also these values are within the limits observed in other titanates and ferrites.

B. Dielectric and Magnetic Properties

The relative permittivity of $Ba_2Fe_2Ti_4O_{13}$ was found to be approximately 28 in the frequency range 7.2–10.8 GHz; the sample exhibited TE_0 resonance at 10.34 GHz with a loss tangent of $2(\pm 1) \times 10^{-3}$. The dielectric loss was moderately dispersive and varied from a value ~0.01 for the loss tangent at 128 MHz to the aforementioned value at 10.34 GHZ.

$Ba_2Fe_2Ti_4O_{13}$ was found to display complex paramagnetic behavior and not to follow the Curie Law. As seen in Fig. 3, the compound exhibits significant field dependence of the mass magnetization with no magnetic satura-

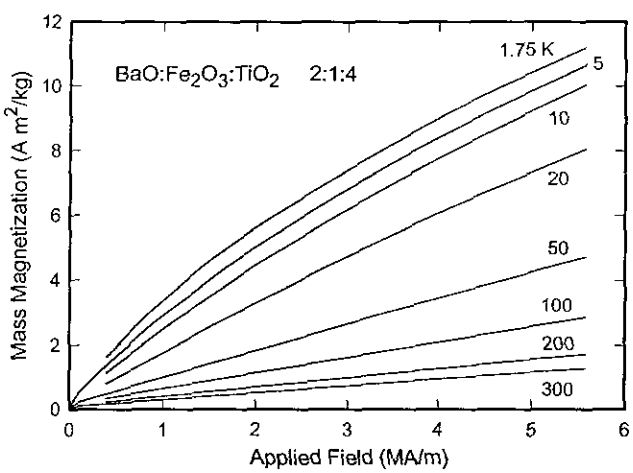

FIG. 3. Mass magnetization vs applied field for $Ba_2Fe_2Ti_4O_{13}$ as a function of temperature showing "ferromagnetic-like" field dependence. No magnetic saturation is observed at any temperature. A distinct change in slope is observed near the origin, especially at 50 K and below; below 0.08 MA/m hysteresis is observed (these data are not shown in the figure).

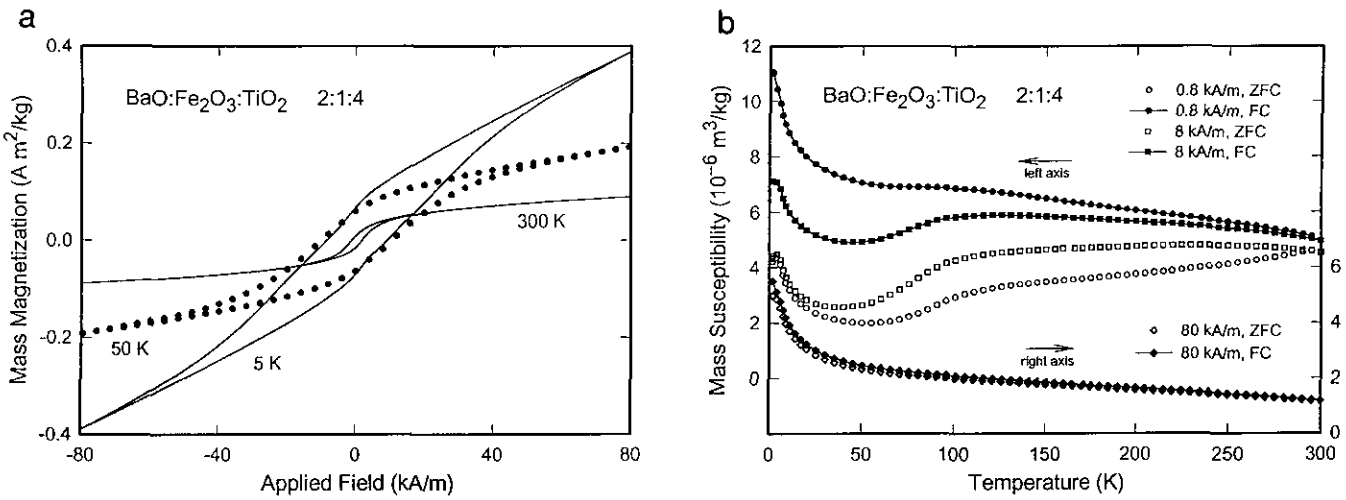

FIG. 4. Hysteresis loops and mass susceptibility curves indicating weak collective behavior in $Ba_2Fe_2Ti_4O_{13}$. (a) Hysteresis loops at 300, 50, and 5 K. Data points are shown only for the 50 K run for clarity. Magnetization and hysteresis decrease markedly with increasing temperature. (b) Mass susceptibility as a function of increasing temperature after zero-field cooling (ZFC, open symbols) and field cooling (FC, filled symbols). (To convert susceptibility values in units of m^3/kg to emu/g, multiply by $10^3/4\pi$.) For 80 kA/m, the data have been shifted down for clarity (right axis scale). *At the highest field (80 kA/m), the exchange interactions are overcome, hence the ZFC and FC data nearly coincide.*

tion observed at any temperature. At 300 K the magnetization at 80 kA/m is 0.088 A · m^2/kg and several orders of magnitude smaller than that of most ferrites. The intrinsic coercivity is 1.5 kA/m. The high-field mass susceptibility, calculated as the slope of the magnetization curve at 300 K, is 2.14×10^{-7} m^3/kg.

Hysteresis loops and mass susceptibility curves indicating collective magnetic behavior in $Ba_2Fe_2Ti_4O_{13}$ are shown in Fig. 4. Hysteresis is minimal above 300 K as seen in Fig. 4a; further, at 80 kA/m the ZFC and FC mass susceptibility vs temperature curves are nearly coincident, as seen in Fig. 4b. As noted previously, no magnetic long range ordering of the iron moments was observed in the neutron experiment down to a temperature of 13 K. The magnetization measurements, however, show that short range correlations exist even at room temperature, although the spin–spin interactions are insufficiently strong to cause long range magnetic ordering. The disorder of the Fe and Ti ions is obviously a factor hindering the development of such ordering.

CONCLUSION

The compound $Ba_2Fe_2Ti_4O_{13}$ has been newly prepared and its crystal structure determined by single-crystal X-ray diffraction and neutron powder diffraction. $Ba_2Fe_2Ti_4O_{13}$ was found to be isostructural with $K_2Ti_6O_{13}$ and $Ba_2ZnTi_5O_{13}$; Fe^{3+} and Ti^{4+} are partially ordered in distorted octahedral sites with barium occupying (8 + 3)-coordinated tricapped quadrilateral prisms. The dielectric properties of $Ba_2Fe_2Ti_4O_{13}$ were found to be moderately dispersive with TE_0 resonance observed at 10.34 GHz, relative permittivity ~28. Polycrystalline $Ba_2Fe_2Ti_4O_{13}$ exhibited complex, field-dependent magnetic behavior. The neutron diffraction studies detected no magnetic ordering down to 13 K; however, magnetization measurements as a function of field and temperature clearly indicate the presence of relatively weak exchange interactions.

REFERENCES

1. R. S. Roth, C. J. Rawn, C. G. Lindsay, and W. Wong-Ng, *J. Solid State Chem.* **104,** 99 (1993).
2. I. E. Grey, A. Collomb, and X. Obradors, *J. Solid State Chem.* **91,** 131 (1991).
3. F. Haberey and M. Velicescu, *Acta Crystallogr. B* **30,** 1507 (1974).
4. X. Obradors, A. Collomb, J. Pannetier, A. Isalgue, J. Tejada, and J. C. Joubert, *Mater. Res. Bull.* **18,** 1543 (1983).
5. C. G. Lindsay, C. J. Rawn, and R. S. Roth, *Powder Diffraction,* **9,** 56 (1994).
6. D. T. Cromer and J. T. Waber, "International Tables for X-Ray Crystallography," Vol. IV, Table 2.2B. Kynoch Press, Birmingham, UK, 1974.
7. A. C. Larson and R. B. VonDreele, "General Structure Analysis System," Report LA-UR-86-748. Los Alamos National Laboratory, Los Alamos, NM 87545, 1990.
8. W. Xi, W. R. Tinga, W. A. G. Voss, and B. Q. Tian, *IEEE Trans. Microwave Theory Tech.* **40,** 228 (1992).
9. W. E. Courtney, *IEEE Trans. Microwave Theory Tech.* **18,** 476 (1970).
10. R. G. Geyer, J. Mantese, and J. Baker-Jarvis, *NIST Tech. Note* 1371 (1994).
11. R. B. Goldfarb and F. R. Fickett, *NBS Spec. Publ. U.S.* 696, (1985).
12. H. Cid-Dresdner and M. J. Buerger, *Z. Kristallogr.* **117,** 411 (1962).
13. N. E. Brese and M. O'Keeffe, *Acta Crystallogr. B* **47,** 192 (1991).
14. D. E. Cox, A. R. Moodenbaugh, J. J. Hurst, and R. H. Jones, *J. Phys. Chem. Solids* **49,** 47 (1988).